Kerbala Journal for Engineering Science

https://kjes.uokerbala.edu.iq

Numerical simulation of the heat transfer characteristics of a thermosyphon heat pipe with different tilt angles and filling ratios

*Ali Hakim Mathry, **Fadhel N. Al-Mousawi, ***Nabeel S. Dhaidan, Ahmed A Alammar****
* Department of Mechanical Engineering, College of Engineering, University of Kerbala, Karbala, Iraq
*E-mail: alisonhakim@yahoo.com
** Department of Mechanical Engineering, College of Engineering, University of Kerbala, Karbala, Iraq.
**E-mail: fadhelnor@gmail.com
*** Department of Mechanical Engineering, College of Engineering, University of Kerbala, Karbala, Iraq.
***E-mail: nabeel.sh@uokerbala.edu.iq
****Centre for sustainable cooling, school of chemical engineering, University of Birmingham
****E-mail: a.a.g.alammar@bham.ac.uk

Received: 18 October 2023; Revised: 12 November 2023; Accepted: 06 December 2023.

Abstract

Computational Fluid Dynamic modeling of a heat pipe can be utilized for investigating the complex physical phenomena of phase change process during the evaporation and condensation in thermosyphon heat pipes. In this study, FLUENT (ANSYS 22) was used to perform a numerical simulation of two-phase flow inside a thermosyphon heat pipe to investigate the effect of both the filling ratio and the inclination angle of the heat pipe on the thermal performance in terms of thermal resistance and temperature distribution. The results were compared with a published research, displaying a good agreement with a highest deviation in the temperature distribution of about 6.3%. According to the results, at a filling ratio of 65%, the average temperature of the evaporator walls was at its lowest, while at a filling ratio of 25%, it was at its highest. At all values of heat input, the lowest total thermal resistance was attained at a tilt angle of 90° and a filling ratio of 65%. Thermal resistance decreases as the heat input increases, and the effects of the filling ratio and tilt angle also become more significant as the heat input rises. Additionally, at a heat input of 400 W, a filling ratio of 65%, and a tilt angle of 90°, the bubbles begin to form at time 1 second, and the vapor rises to the condenser section starting at time 20 second, carrying with it the thermal energy. While condensation begins at time 27 second.

Keywords: Numerical Simulation, Heat Pipe, Thermosyphon, Filling Ratio, Tilt Angle.

Nomenclature	
CFD	Computational Fluid Dynamic
HPs	Heat pipes
VOF	Volume of fluid
α_L	Volume fraction of liquid
α_V	Volume fraction of vapor
u	Velocity of fluid
ρ	Density of fluid
μ	Viscosity of fluid
Q'	Heat flux
Q	Heat input
A_{lm}	Logarithmic mean cross-section
T_m	Mean temperature of the cooling water
$T_{cw,av}$	Condenser's average wall temperature
Q_{cond}	Heat extracted from the condenser
T_{in}	Temperatures at the cooling water's intake
T_{out}	Temperatures at the cooling water's discharge

1.Introduction

Heat pipes are devices that transfer heat from one location to another through the evaporation and condensation of a working fluid contained within a closed container **[1]**. The main sections of heat pipes are the evaporator and condenser, where heat is received in the evaporator section from the heat source and rejected in the condenser to the heat sink. The working fluid evaporates in the evaporator section, and the vapor moves to the condenser section, where the condensate loses its latent heat. In the case of a wickless heat pipe (thermosyphon), the condensate returns to the evaporator section by gravity and by capillary force in the case of a wicked heat pipe **[2].** Heat pipes are utilized in a variety of applications, such as in solar thermal technologies **[3, 4]**, heat dissipation of electronic components **[5]**, geothermal

energy utilization **[6],** air conditioning systems **[7]**, etc. This is because of flexibility in operation and application, compact design, being very efficient in transporting heat even under small temperature differences, not requiring external power, and other advantages **[8]**. Due to its straightforward design and affordable price, wickless heat pipe (thermosyphon) has attracted a lot of attention. Many researchers have conducted practical experiments and numerical studies to improve the thermal performance of a thermosyphon by studying the effects of a number of variables that can enhance thermal performance of the thermosyphon, such as the title angle and filling ratio.

Noie **[9]** experimentally studied the influence of filling ratio on the performance of thermosyphon heat pipe under different values of aspect ratio (length of evaporator to its diameter). Three different filling ratios (30%, 60%, and 90%) were used with three aspect ratios (11.8, 9.8, and 7.45). According to the results, the maximum heat transfer rate for each aspect ratio depends on the filling ratio. The highest heat transfer rate was obtained for the aspect ratio of 11.8 at a filling ratio of 60%, while it occurs at a filling ratio of 30% and 90% for both aspect ratios of 9.8 and 7.45, respectively. J. Raghuram **[10]** experimentally and numerically studied the effect of tilt angle on the performance of the thermosyphon heat pipe. The dimensions of the heat pipe are 12 mm in diameter and 300 mm in length. The acetone and distilled water were used as a working fluid with a filling ratio of 20%, a heat input value of 7.29 W, and five angles of inclination (0°, 30°, 45°, 60°, and 90°). The results demonstrated that, in both cases (using water or acetone), the highest value of thermal performance was at a 60° tilt angle. Jiao et al. **[11]** investigated analytically and experimentally the effect of filling ratio on the thermosyphon heat pipe. They used eight small values for the filling ratios (4.5%, 6.37%, 10.1%, 11.8%, 13.5%, 15.2%, 18.5%, and 20.2%) and five values of heat input (5, 10, 15, 20, and 25). According to the results, they concluded that the efficiency of the heat pipe is at its lowest values at small filling ratios (4.5%, 6.37%, and 10.1%) and its highest values at filling ratios (11.8%, 13.5%, and 15.2%). Chehade et al. **[12]** carried out work similar to the previous work, with the difference that the heat pipe used is a loop thermosyphon. They concluded that the ideal filling ratios were between 7% and 10%. Manimaran et al**. [13]** experimentally studied the effect of filling ratio and tilt angle on the thermal resistance of thermosyphon. Four values of filling ratio (25%, 50%, 75%, and 100%) and four of tilt angle (0°, 30°, 60°, and 90°) were used, with different values of heat input (30, 40, 50, 60, and 70W). According to the findings, the 75% filling ratio and vertical orientation resulted in the lowest thermal resistance. Alizadhdakel et al. **[14]** investigated experimentally the effect of filling ratio on the performance of thermosyphon. They conducted a CFD simulation to

examine the influence of the non-condensable gases on phase change events across a thermosyphon and compare the results with those from an experiment. Three filling ratios and three heat inputs (30%, 50%, and 80%) and (350, 500, and 700 W) were used, respectively. According to the results, the best thermal performance of the thermosyphon is at a filling rate of 50%. Lin Lu et al. **[15]** experimentally investigated the effect of the filling ratio on the thermal performance of the thermosyphon. Water and nanofluid were used as working fluids at different filling ratios (40%, 50%, 60%, and 70%). In both cases, when using water or nanofluid, the optimum filling rate was 60%. Halit Arat **[16]** presented an experimental study to examine the impact of the tilt angle on the performance of thermosyphon. The total length of heat pipe was 1500 mm, and the inner and outer diameters were 26 and 28 mm, respectively. The working fluid used is water with four different volume values (5, 10, 15, and 20 ml) and tilt angles of 45°, 60°, and 90°. It was found that the optimum performance was achieved at a 90° tilt angle. It is clear from the aforementioned experimental and numerical studies that the filling ratio and tilt angle for every heat pipe depend on a variety of parameters, including geometry, liquid type, heat input, and operating conditions. The appropriate filling ratio and tilt angle should be determined before the experimental work in order to save time and cost on the research. In this study, a two-dimensional CFD modeling was implemented to study the effects of three various values of filling ratio (25%, 65%, and 100%) of water and tilt angle (30°, 60°, and 90°) on the performance of thermosyphon heat pipe at different values of input power.

2. Governing equations

Numerical simulations based on the Finite Volume Method are more challenging for multiphase flows than for single-phase flows. This issue or challenge calls for a significant processing effort due to the non-stationary nature of the phase transitions and the physical properties like density and viscosity. The volume of fluid approach was applied to solve these issues. The motion of the interfaces was defined indirectly as a result of this computation, assigned computing the motion of all phases.

The VOF approach, which applies surface-tracking to a fixed mesh, allows for the modeling of two-phase fluids with a well-defined interface between the phases. The computational domain of the VOF model solves a specific set of Navier-Stokes equations, and it also tracks the motion of the various phases by specifying the volume fraction of each phase. In another sense, the volume fraction of liquid and the volume fraction of vapor can be anticipated under three of the following conditions **[17]**:

- $\alpha_L = 1$: The liquid has completely filled the cell.

- $\alpha_L = 0$: The vapour has completely filled the cell.
- $0 < \alpha_L < 1$: The cell is at the interface between the vapour and liquid.

At the third case, all phases' volume fractions add up to one.

Equations relating to continuity, momentum, and energy are employed to describe the movement of the working fluid within the heat pipe **[18]**.

2.1 Continuity Equation:

$$\frac{\partial(\rho u)}{\partial x} + \frac{\partial(\rho v)}{\partial y} + \frac{\partial(\rho w)}{\partial z} = 0 \tag{1}$$

2.2 Momentum Equation:

In x-direction is:

$$\rho\left[u\frac{\partial u}{\partial x} + v\frac{\partial u}{\partial y} + w\frac{\partial u}{\partial z}\right] = -\frac{\partial p}{\partial x} + \frac{\partial}{\partial x}\left[(\mu + \mu_t)2\frac{\partial u}{\partial x}\right] + \frac{\partial}{\partial y}\left[(\mu + \mu_t)\left(\frac{\partial u}{\partial y} + \frac{\partial v}{\partial x}\right)\right] + \frac{\partial}{\partial z}\left[(\mu + \mu_t)\left(\frac{\partial u}{\partial z} + \frac{\partial w}{\partial x}\right)\right] \tag{2}$$

In y-direction is:

$$\rho\left[u\frac{\partial v}{\partial x} + v\frac{\partial v}{\partial y} + w\frac{\partial v}{\partial z}\right] = -\frac{\partial p}{\partial y} + \frac{\partial}{\partial y}\left[(\mu + \mu_t)2\frac{\partial v}{\partial y}\right] + \frac{\partial}{\partial x}\left[(\mu + \mu_t)\left(\frac{\partial u}{\partial y} + \frac{\partial v}{\partial x}\right)\right] + \frac{\partial}{\partial z}\left[(\mu + \mu_t)\left(\frac{\partial v}{\partial z} + \frac{\partial w}{\partial y}\right)\right] \tag{3}$$

In z-direction is:

$$\rho\left[u\frac{\partial w}{\partial x}+v\frac{\partial w}{\partial y}+w\frac{\partial w}{\partial z}\right] = -\frac{\partial p}{\partial z}+\frac{\partial}{\partial z}\left[(\mu+\mu_t)2\frac{\partial w}{\partial z}\right]+\frac{\partial}{\partial x}\left[(\mu+\mu_t)\left(\frac{\partial u}{\partial z}+\frac{\partial w}{\partial x}\right)\right]+\frac{\partial}{\partial y}\left[(\mu+\mu_t)\left(\frac{\partial v}{\partial z}+\frac{\partial w}{\partial y}\right)\right] + \frac{\partial}{\partial y}\left[(\mu+\mu_t)\left(\frac{\partial v}{\partial z}+\frac{\partial w}{\partial y}\right)\right] \quad (4)$$

$$\rho = \alpha_l\rho_l + \alpha_v\rho_v \quad (5)$$

$$\mu = \alpha_l\mu_l + \alpha_v\mu_v \quad (6)$$

2.3 ***Energy equation:***

$$\frac{\partial}{\partial x}(\rho uT)+\frac{\partial}{\partial y}(\rho vT)+\frac{\partial}{\partial z}(\rho wT) = \frac{\partial}{\partial x}\left[\left(\frac{\mu}{Pr}+\frac{\mu_t}{\sigma_T}\right)\frac{\partial T}{\partial x}\right]+\frac{\partial}{\partial y}\left[\left(\frac{\mu}{Pr}+\frac{\mu_t}{\sigma_T}\right)\frac{\partial T}{\partial y}\right]+\frac{\partial}{\partial z}\left[\left(\frac{\mu}{Pr}+\frac{\mu_t}{\sigma_T}\right)\frac{\partial T}{\partial z}\right]+SR \quad (7)$$

3 CFD Simulation Set up

3.1 Geometry

A workbench (ANSYS Fluent 2022) has been used to build the geometry of a thermosyphon in the vertical plane in two dimensions. The geometry of a copper tube is shown in Fig. 1**,** copper is chosen for several reasons, the most important of which is its high conductivity, which reaches 397 W/m K**.** This tube has an inner diameter and wall thickness of Ø22.4 mm and 0.8 mm, respectively. The length of the tube measures 480 mm from the beginning of the edge to the end of the edge. The thermosyphon includes an evaporator section that is 200 mm in height, an adiabatic section that is 80 mm in height, and a condenser section that is 200 mm in height.

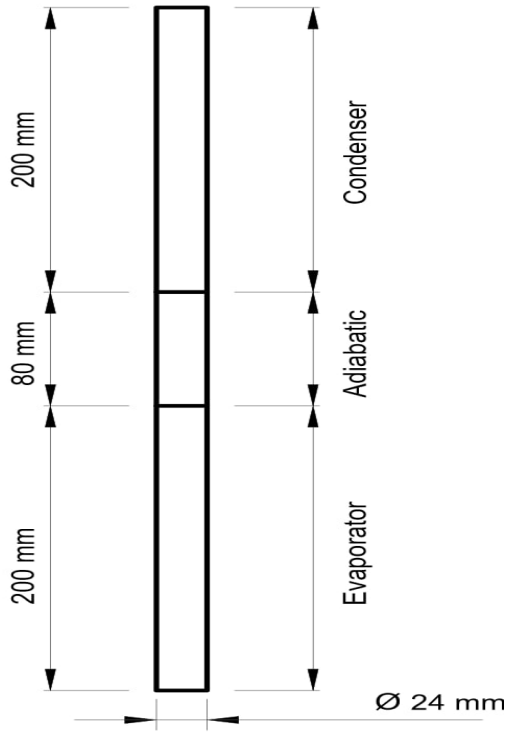

Figure 1. Heat pipe 2D geometry adopted in this study.

3.2 Meshing

Using the Workbench module of ANSYS Fluent 2022, the geometry has been meshed. The grid was managed using the method of controlling edge sizing across all domains. A bias factor of (5) is applied to regulate cell sizes near inner walls and within the solid domain (walls) in order to effectively capture the flow and heat transfer in these locations**.** As can be seen in Fig. 2, which illustrates the lower 300 mm portion with wall mesh, three alternate structured mesh sizes were generated in order to evaluate the solution's sensitivity to mesh size. These sizes consisted of 8340, 12540, and 20790 elements, respectively.

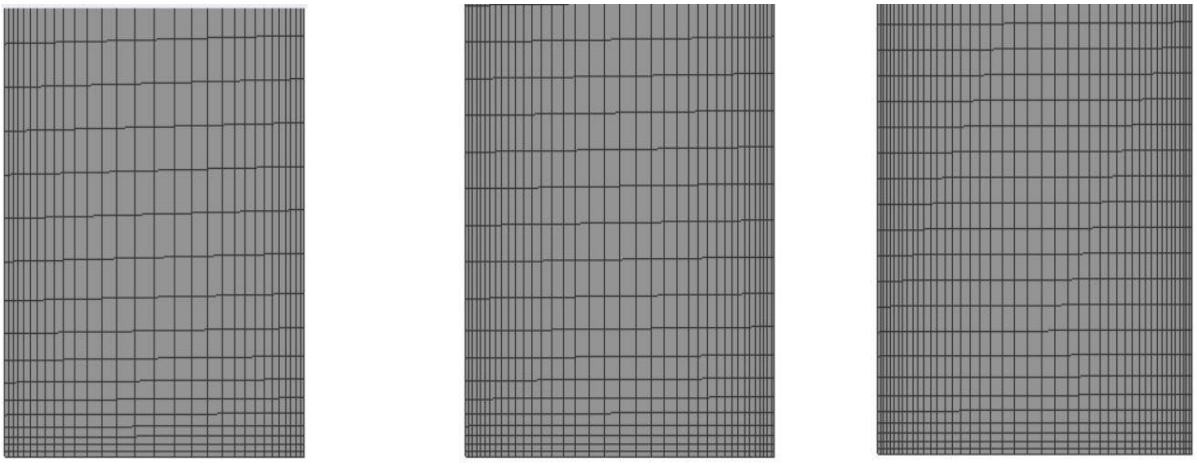

Figure 2. Different Mesh Sizes of 8340 elements, 12540 elements, and 20790 elements.

3.3 Grid independence test

Fig. 3 shows the temperature distribution along the heat pipe's wall for a variety of computational cell sizes when subjected to a heat input of 100 W and a filling ratio of 100%. It is noted that when a mesh has a number of 12540 and 20790 elements, the temperatures are similar in the two cases, while they differ with a relative increase in the case of choosing a network with 8340 elements than in the previous two cases. This is shown by the data. As a result, a mesh size of 12540 elements is utilized in this study to reduce the amount of computing time required for the solution without compromising the level of precision achieved.

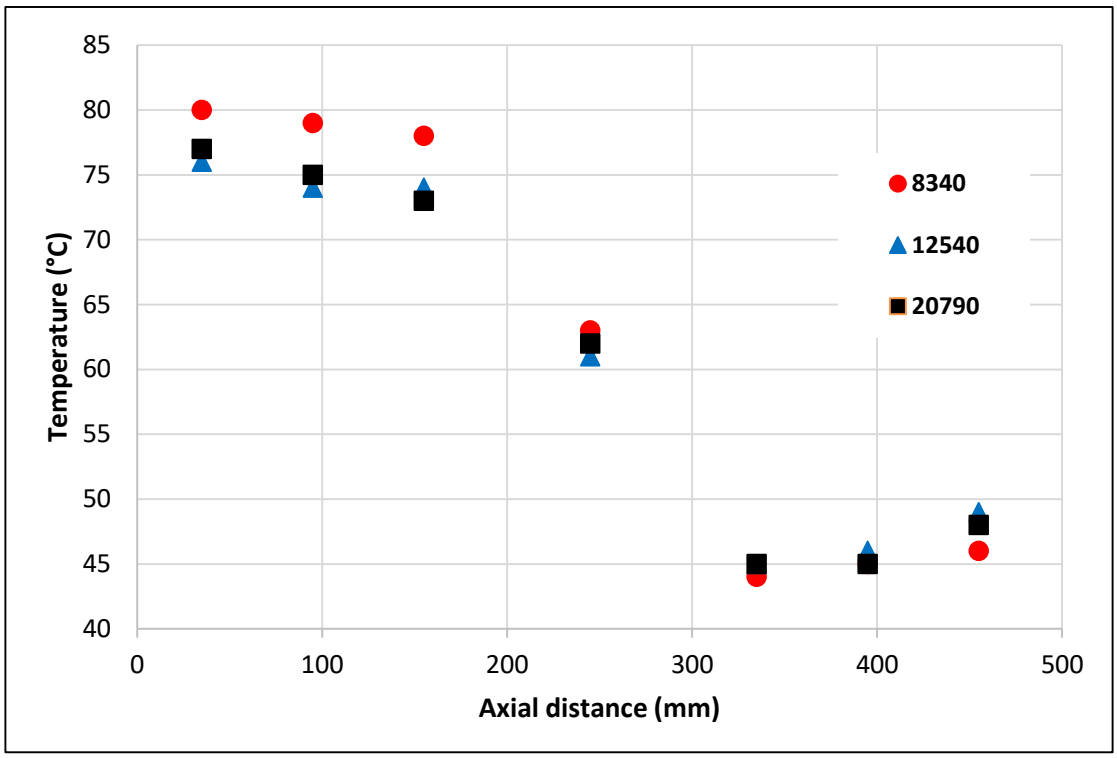

Figure 3. Grid independence test.

3.4 Operating and Boundary conditions

In this study, three different filling ratios (25%, 65%, and 100% of the evaporator volume) and three inclination angles (30°, 60°, and 90°) are utilized. The heights of the evaporator that correspond to these filling ratios and inclinations are initially patched with liquid, and the heights that remain are filled with vapor. The tilt angle was set by multiplying the y-component of the gravity acceleration by the sine of the angle and then multiplying the x-component of the gravity acceleration by the cosine of the angle. This can be seen in Fig. 4. Three distinct filling ratios and tilt angles are utilized, specifically 25%, 65%, and 100% of the evaporator volume, and 30º, 65º, and 90º, respectively. In order, the relevant evaporator height is initially patched with liquid in order to establish the filling ratio for each situation, and after that, vapor is applied to the remaining height. Additionally, the tilt angle is referred to as the angle at which the thermosyphon is tilted with respect to the horizontal axis.

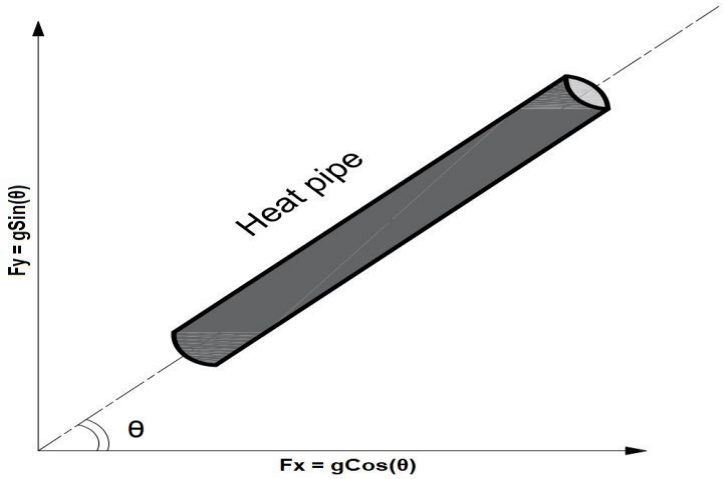

Figure 4. Tilt angle of thermosyphon heat pipe.

The simulation started with the evaporator wall and liquid at 100^{o}C (same value of the boiling point), and we started the simulation with the condenser wall at 20^{o}C (same value of cooling water at the water jacket temperature). This allowed us to reduce the amount of time it took for the simulation to run. When working with an ideal gas, the system's lowest temperature should be used as the operating temperature, which in this case is 20^{o}C. Similarly, when working with constant gas density, the operating density should be set to the lowest density in this case. In addition, we decided that the saturation temperature would be 100^{o}C, and the working pressure would be 101325 Pascals **[19]**.

The boundary condition was non-slip to the interior walls of the condenser, evaporator, and adiabatic, and a constant heat flux (Q") was imposed on the outside evaporator wall to represent the heat source for the thermosyphon. A non-slip boundary condition was applied to the inner walls of the condenser, evaporator, and adiabatic section. In order to account for the fact that the temperature distribution caused by radial conduction through a cylindrical wall is logarithmic rather than linear, four different values of heat flux were utilized: 9804, 19608, 29412, and 39216 W/m^2. These values corresponded to heat transfer rates of 100, 200, 300, and 400 W, respectively. To do this, the heat input (Q) was divided by the area of the logarithmic mean cross-section (A_{lm}) using the formulae described in **[20].**

$$Q'' = \frac{Q}{A_{lm}} \tag{8}$$

$$A_{lm} = \frac{A_{\text{outer}} - A_{\text{inner}}}{\ln\left(\frac{A_{\text{outer}}}{A_{\text{tinne}}}\right)} \tag{9}$$

$$A_{lm}\& = \frac{2\pi r_{\text{outer}} L - 2\pi r_{\text{inner}} L}{\ln\left(\frac{2\pi r_{\text{outer}} L}{2\pi r_{\text{inner}} L}\right)} \tag{10}$$

$$A_{lm} = 2\pi L \left(\frac{r_{\text{outer}} - r_{\text{inner}}}{\ln \frac{r_{\text{outcr}}}{r_{\text{tiner}}}} \right) \tag{11}$$

The walls of the thermosyphon's insulated bottom and top ends did not experience any cooling or heating. The wall of the adiabatic section is defined with a heat flux value of zero. On the other hand, On the walls of the condenser section, convection boundaries are inserted to simulate heat transfer through the cooling water. Therefore, the following equation must be used to determine the heat transfer coefficient from the condenser's wall to the cooling water **[9]**.

$$h_{\text{conv}} = \frac{Q_{\text{cond}}}{\pi D L_{\text{cond.}} \left(T_{cw,av} - T_m\right)} \tag{12}$$

All parameters of equation 12 The condenser's average wall temperature ($T_{cw,av}$), the mean temperature of the cooling water (T_m), and heat extracted from the condenser (Q_{cond}) were obtained from experimental work and utilized to determine the convective heat transfer coefficient for each case and feed them into Ansys fluent for this study.

$$T_{cw,av} = \frac{T_{33} + T_{39} + T_{46}}{3} \tag{13}$$

$$T_m = \frac{T_{\text{in}} + T_{out}}{2} \tag{14}$$

Where T_{33}, T_{39}, and T_{46} are the temperatures at 0.33, 0.39, and 0.46 m from the condenser's wall. Temperatures at the cooling water's intake and discharge are denoted by "T_{in}" and "T_{out}" respectively.

3.5 Solution Techniques and Methods

In this study, used the VOF method to model multi-phase flow, and a body force term was included by activating the gravitational force of 9.81 m/s^2. As a secondary phase (liquid phase), water was selected, and its density was determined to be a function of temperature (T) according to the following relation **[21]**:

$$\rho_l = 859.0083 + 1.252209T - 0.0026429T^2 \quad (15)$$

Fig. 5 shows the flow chart of heat pipe simulation. Because of the unpredictable nature of the two-phase flow **[22]**, a transient solution with a time step of 0.01s was used in all instances. For computations of momentum and energy as well as pressure-velocity coupling, in computational fluid dynamics (CFD), the SIMPLE algorithm and the first-order upwind approach are employed, respectively **[14]**. Geo-Reconstruct and PRESTO discretization were chosen **[23]** for calculating the volume fraction and pressure, respectively. When the residuals for the velocity and mass components are less than (10-4) and the residuals for the temperature-dependent variables are less than (10-6**) [19].**

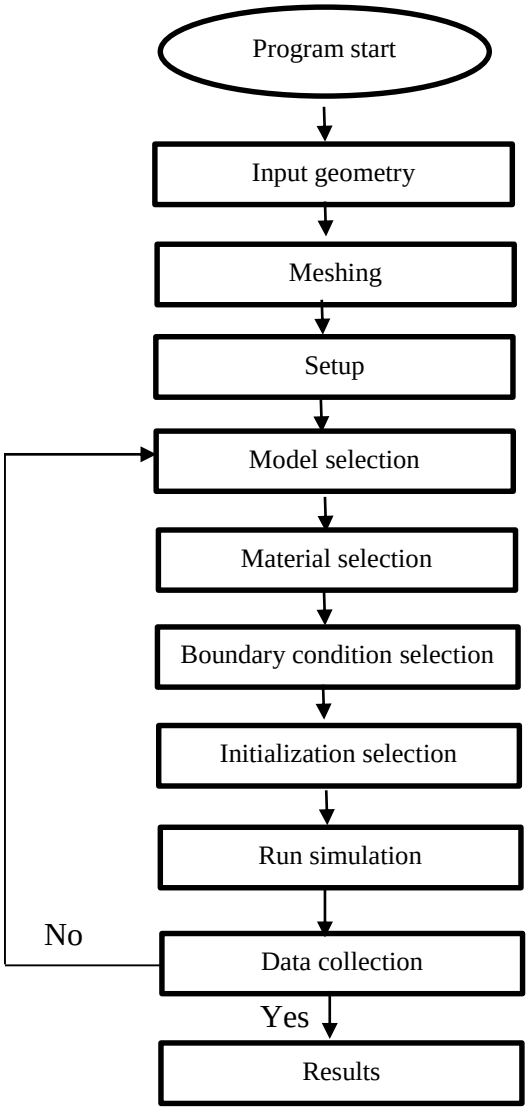

Figure 5. flow chart of heat pipe simulation.

4. Results and Discussion

4.1 Validation of the CFD solution

The same geometry and boundary conditions for heat pipe simulations employed by Alammar et al. **[19],** have been used to support the current CFD simulation. The CFD results have been compared with the those of Alammar et al. [19] to determine the temperature distribution along the thermosyphon wall, as shown in Fig. 6. The power input of 101 and 39 W with a 100% filling ratio and tilt angle of 90° examined for the numerical work of thermosyphon heat pipe by Alammar et al. **[19]** were used for the CFD modeling of the present work. The CFD solution was found to have a good agreement with the Alammar et al. [19]'s study. However, for 39 W of heat input, a maximum deviation of 6.3% was found in the condenser's upper region. And for 101 W of heat input, a maximum deviation of 4.3% was found in the central region of the evaporator section.

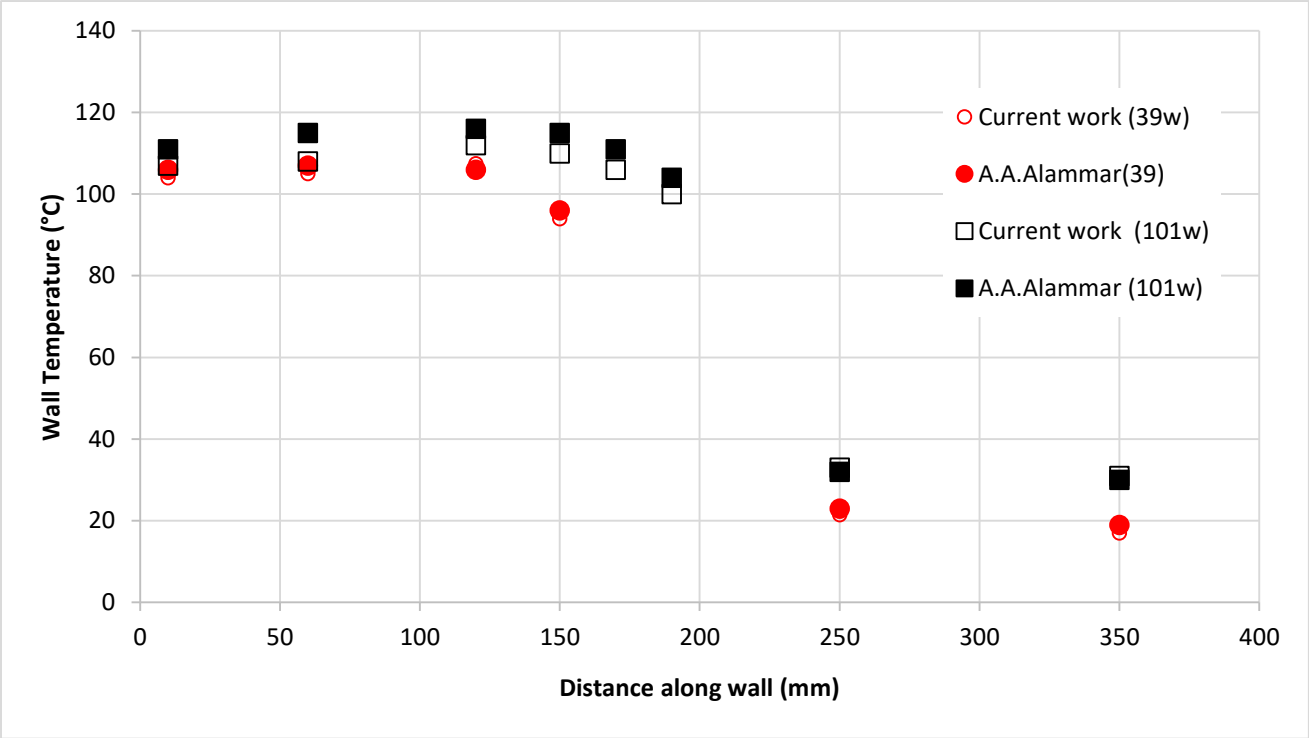

Figure 6. Comparison of temperature distribution along the wall of thermosyphon between A.A.Alammar numerical study data [19] and CFD results of the current work.

4.2. Filling ratio effect

A CFD simulation was used to obtain the impact of the filling ratio on the performance of thermosyphon. Therefore, the distribution of temperature on the wall of the thermosyphon for filling ratios (25%, 65%, and 100%) is shown in Fig. 7 at an input power of 400W and a tilt angle of 90°. Fig. 6 shows similar trends in the distribution of temperature along the thermosyphon's wall for all filling ratios. Also, it is noted that the effect of changing the filling ratio on the profile of temperature is more significant in the evaporator than in the condenser. Additionally, at a filling ratio of 65%, the lowest wall temperature distribution is seen, and the maximum temperature profile is seen at a filling ratio of 25%. On the other hand, the temperature profile along the evaporator section is similar at a high filling ratio of 100% compared to other filling ratios. This is because all evaporator sections fall within the working fluid region. In the condenser section, the temperature of the lower region of the condenser is less than that of the higher region of the condenser for a filling ratio of 65%. While the temperature of the condenser is similar at filling ratios of 25% and 100%.

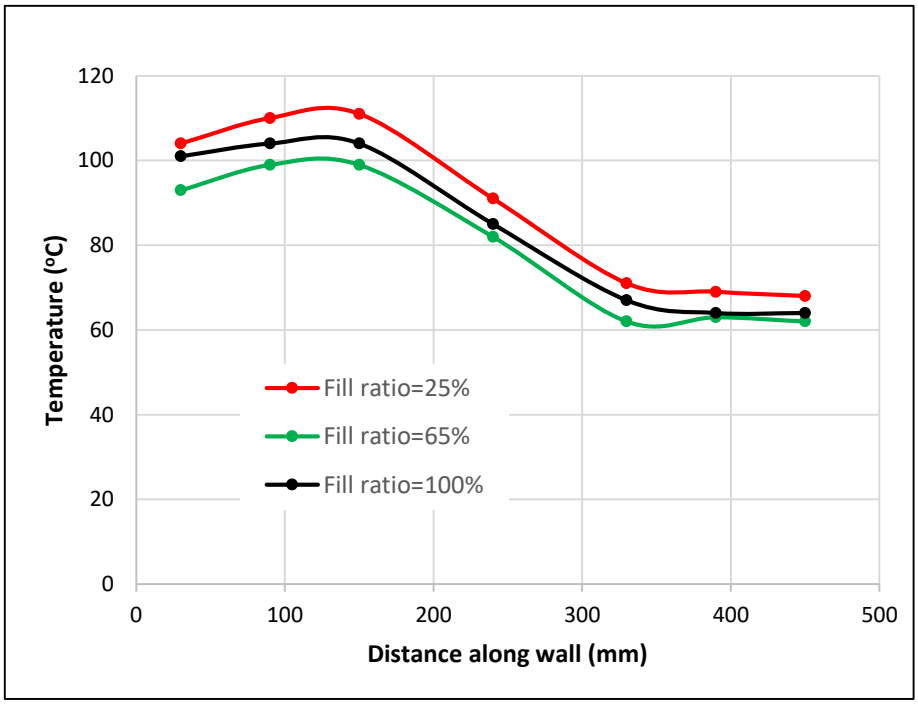

Figure 7. Temperature distribution along heat pipe wall for various filling ratio, tilt angle of 90° and heat input of 400W.

Fig. 8 shows the impact of the filling ratio on the evaporator section's average wall temperature for four different heat input values (100, 200, 300, and 400 W) at a tilt angle of 90°. According to the results, the average temperature of the evaporator walls decreases from its highest value at 25% filling ratio to its lowest value at 65% filling ratio, then rises again at 100% filling ratio for heat inputs of 300 and 400 W (**[12]** observed the same trend). However, at values of heat input of 100 and 200 W, there is a small variation in the wall temperature of the evaporator between all filling ratios, especially between filling ratios (25% and 100%). Consequently, with relatively high input power (300 and 400 W), the influence of filling ratio on evaporator wall temperature is more apparent than that at low input power (100 and 200 W).

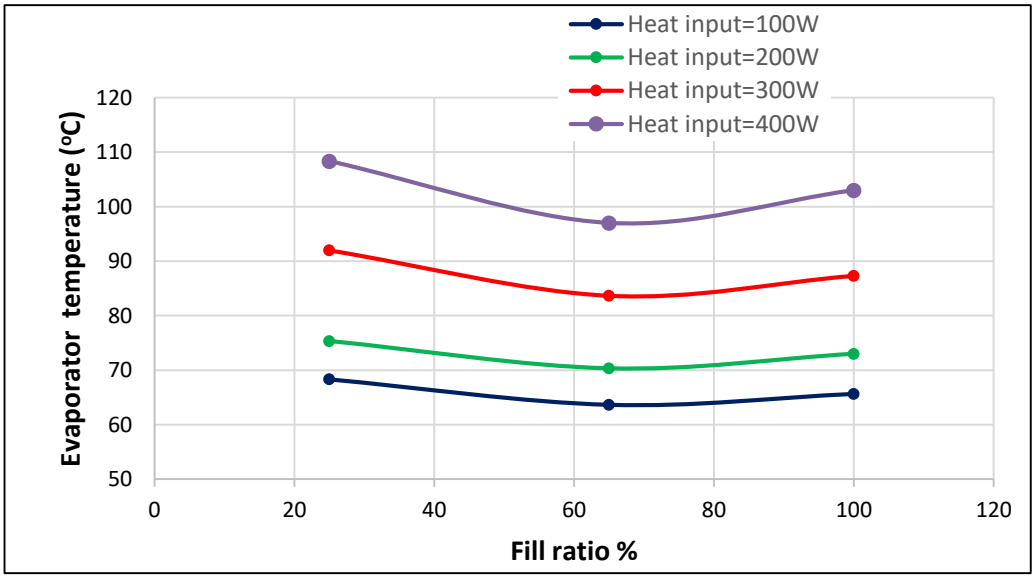

Figure 8. Variation in the evaporator's average wall temperature with filling ratio at various heat inputs (tilt angle of 90°).

Fig. 9 shows the impact of filling ratio on thermal resistance for different input power. For three different filling ratios (25%, 65%, and 100%) and a tilt angle of 90°, it can be shown that the thermal resistance falls down as the power input rises. Due to the small amount of working fluid present at a filling ratio of 25% for any power input, a greater thermal resistance is seen, while a lower value at 65% for all power inputs (**[13] observed the** same trend) at a filling ratio of 25% shows a higher thermal resistance. This indicates that with low filling ratios, the thermosyphon has reached its heat transfer limit, which led to high temperatures at the upper region of the evaporator, as shown in Fig. 1, while at a 65% filling ratio, the thermal resistance is lower for all input powers. At a power input of 400 W, the gap in thermal

resistance across the 25% and and100% filling ratios narrows significantly. But in general, for input power (100, 200, 300, and 400W), a filling ratio of 65% is the best case, according to this study. This is because the charge of the working fluid is determined by a combination of two factors: Dehydration occurs when fluid intake is inadequate. Condensation in the condenser is hindered if too much fluid is delivered to it, which can happen if the fluid level is too high. Therefore, the first factor applies to 25%, while the second consideration applies to 100% of the filling ratio. Since there is no dryness from the low amount of liquid or surface blockage from an increase in liquid, a filling ratio of 65% is optimal, according to this study. This agrees with the findings of, which found that a filling ratio of 65% is optimal **[25]**.

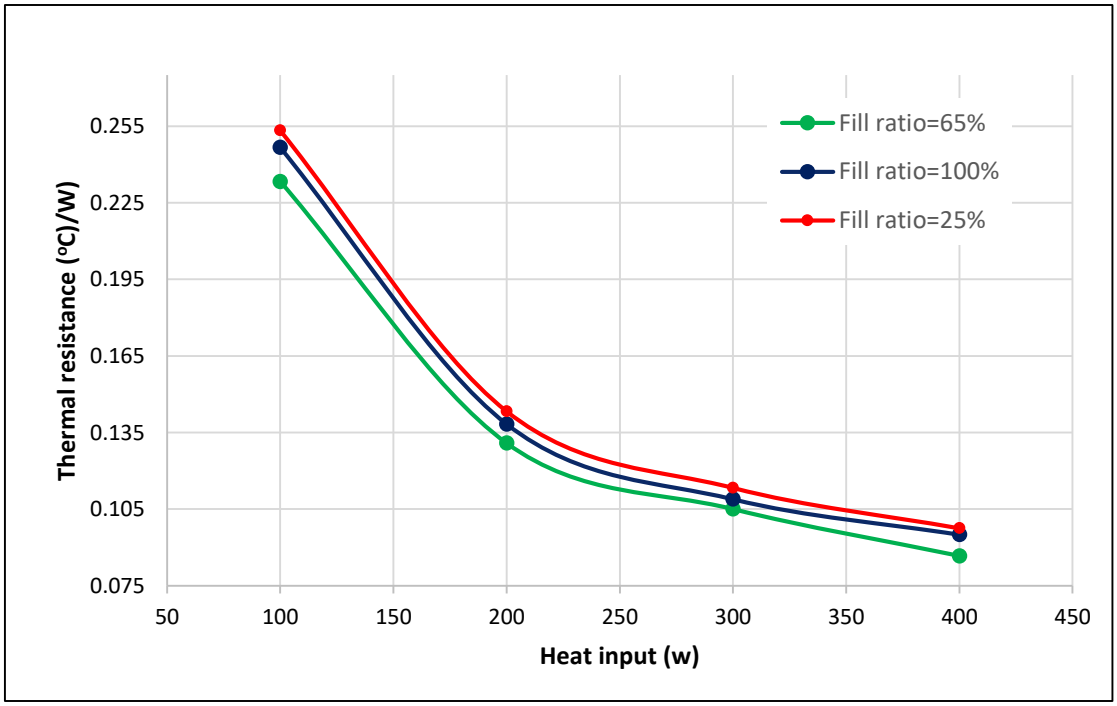

Figure 9. Thermal resistance variations with power input for heat pipe wall for different filling ratios and tilt angle of 90°.

4.3 Effect of inclination angle

Fig.10 shows the temperature distribution along the heat pipe for three various angles of inclination (30°, 60°, and 90°), an input power of 400 W, and a filling ratio of 65%. Due to the considerable thickness of the condenser layer caused by the fast evaporation rate at inclination angles of 90°, the upper region of the condenser is significantly higher than the lower region. At an angle of 90°, the condenser average temperature rises as high as it can, and it rises by a smaller value at 60° and 30°. On the other hand, it is

noted that the highest temperature of the evaporator is at an angle of 30°. The reason for higher temperatures at low angles of inclination is attributed to the fact that some of the upper part of the evaporator section is not in touch with liquid due to low inclination degrees.

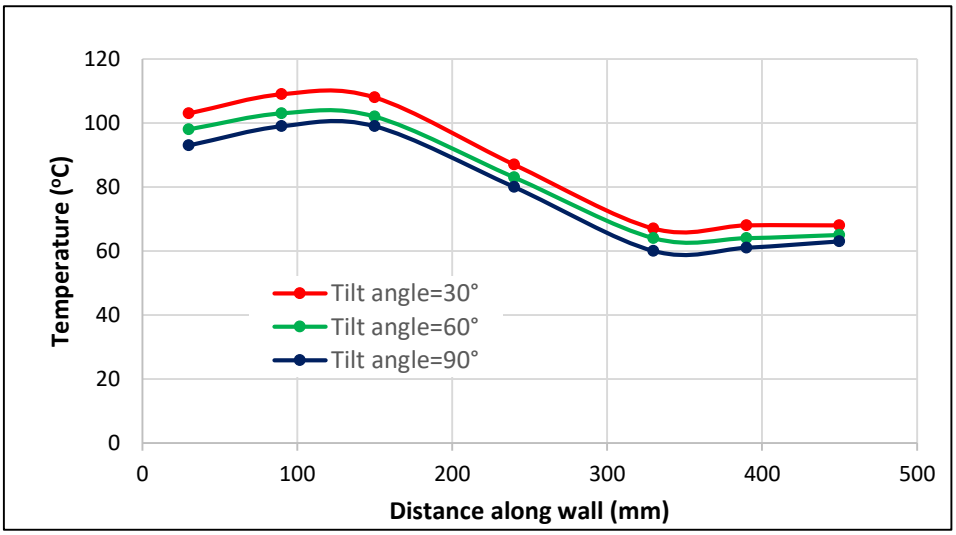

Figure 10. Temperature distribution along heat pipe wall for various angles of inclination, filling ratio of 65% and input power of 400W

Fig. 11 shows the total thermal resistance against heat input of the grooved heat pipe at three different tilt angles (30°, 60°, and 90°) with a filling ratio of 65%. It was found that as input power was increased, the thermal resistance decreased. The total thermal resistance also depends on the heat pipe's inclination angle. and the results show that the overall thermal resistance of the heat pipe is lower at a tilt angle of 90° compared to 60° and 30°. Since the evaporator section can maintain the full effect of gravity by returning the condensed vapor to the evaporator section, 90° is the optimal inclination compared to 60° and 30° (similar conclusions were reported by **[13, 24]**).

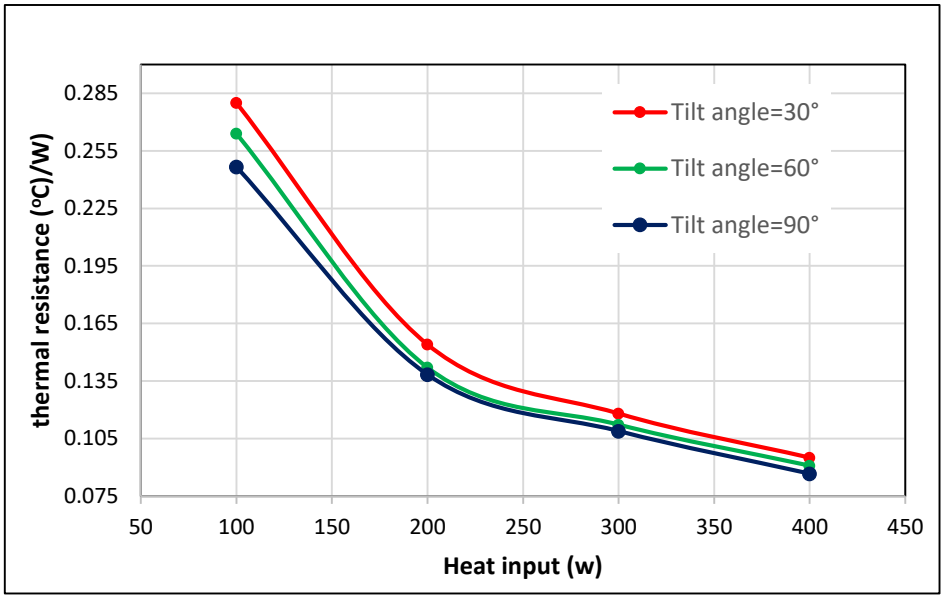

Figure 11. Thermal resistance variations with power input for heat pipe wall at various angles of inclination and filling ratio of 65%

4.5 Flow Visualization of CFD Simulation

Fig.12 shows the contrast of the vapor volume fraction with time of simulation at a power input of 400 W, a filling ratio of 65% of the evaporator volume, and a tilt angle of 90°. When only vapor is present, the color is red (vapor volume fraction = 1), but when only liquid is present, the color is blue (vapor volume fraction = 0). It is seen that at 1 s, bubbles begin to form as a result of the working fluid reaching the boiling point. These bubbles begin to increase in size as a result of increased heating at (5–10) s and rise to the surface of the liquid. Then at the second (20), the volume fraction of the vapor increases and rises to the condenser section and carries thermal energy with it to the condenser, and this continues, and then the steady state condition at time 30 s. Then this rising vapor condenses on the walls of the condenser, starting at the 27th second, to produce a layer of condensing liquid in a time of 30 s, as shown in Fig.13.

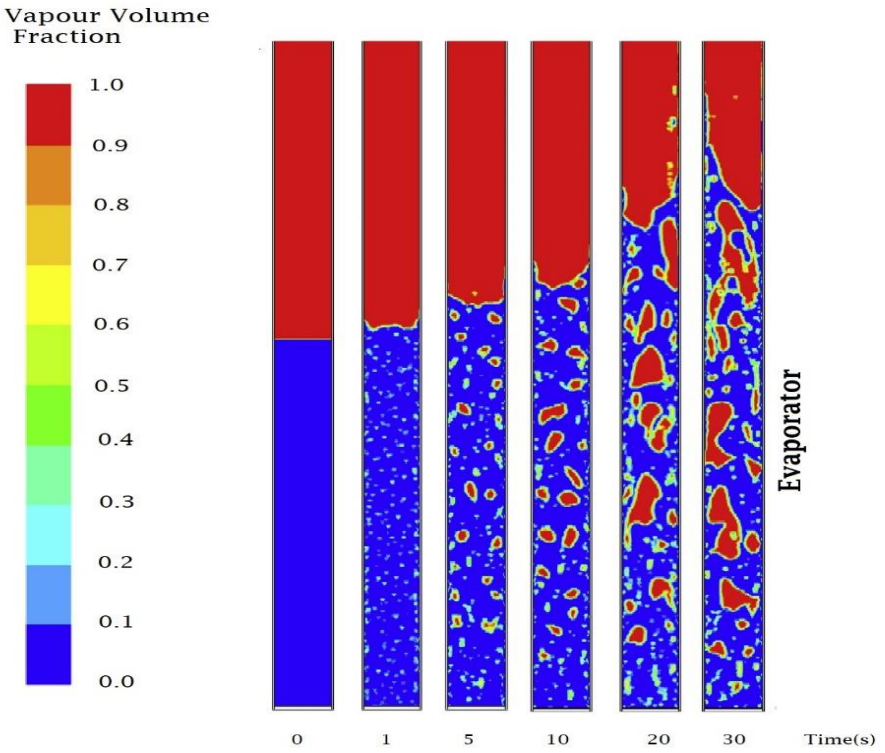

Figure 12. Vapour volume fraction contours at various simulation times (400W input power, 65 % filling ratio and 90° tilt angle).

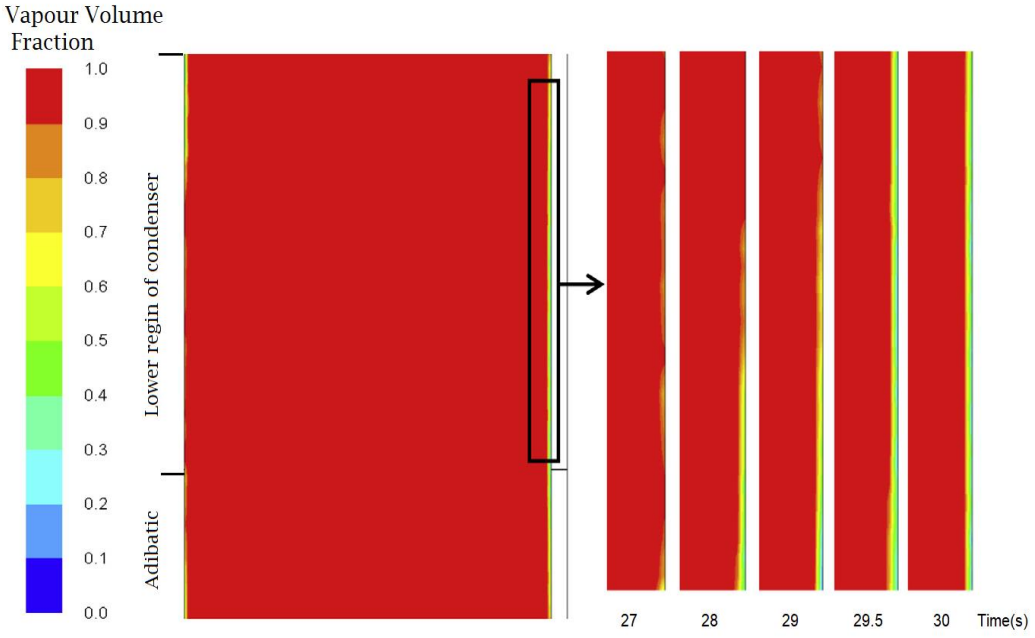

Figure 13. Contours of volume fraction of condensed liquid film in the lower region of condenser at different times.

During the thermosyphon process (the thermosyphon process is a method of passive heat exchange based on natural convection that operates in a two-phase cycle **[25]**), at a power input of 400 W, filling ratio of 65%, and tilt angle of 90°, the temperature profiles were recorded. As can be seen in Fig. 5.28 (0.5 s to 3 s), initial increases in evaporator temperature resulted from the application of heating power; the phase change started when the evaporator section temperature hit the boiling point. while at (3 s to 5 s), the vapor moves over the adiabatic section to the condenser section as the heating power in the evaporator section continues. Once the vapor reaches the condenser section, as shown in Fig.14 (10 s), a high-temperature area develops there. The vapor condenses to liquid as its high temperature in the condenser portion drops, and the liquid then returns to the evaporator section thanks to gravity. After that period, the thermosyphon's internal temperature becomes consistent throughout 15 to 30 s.

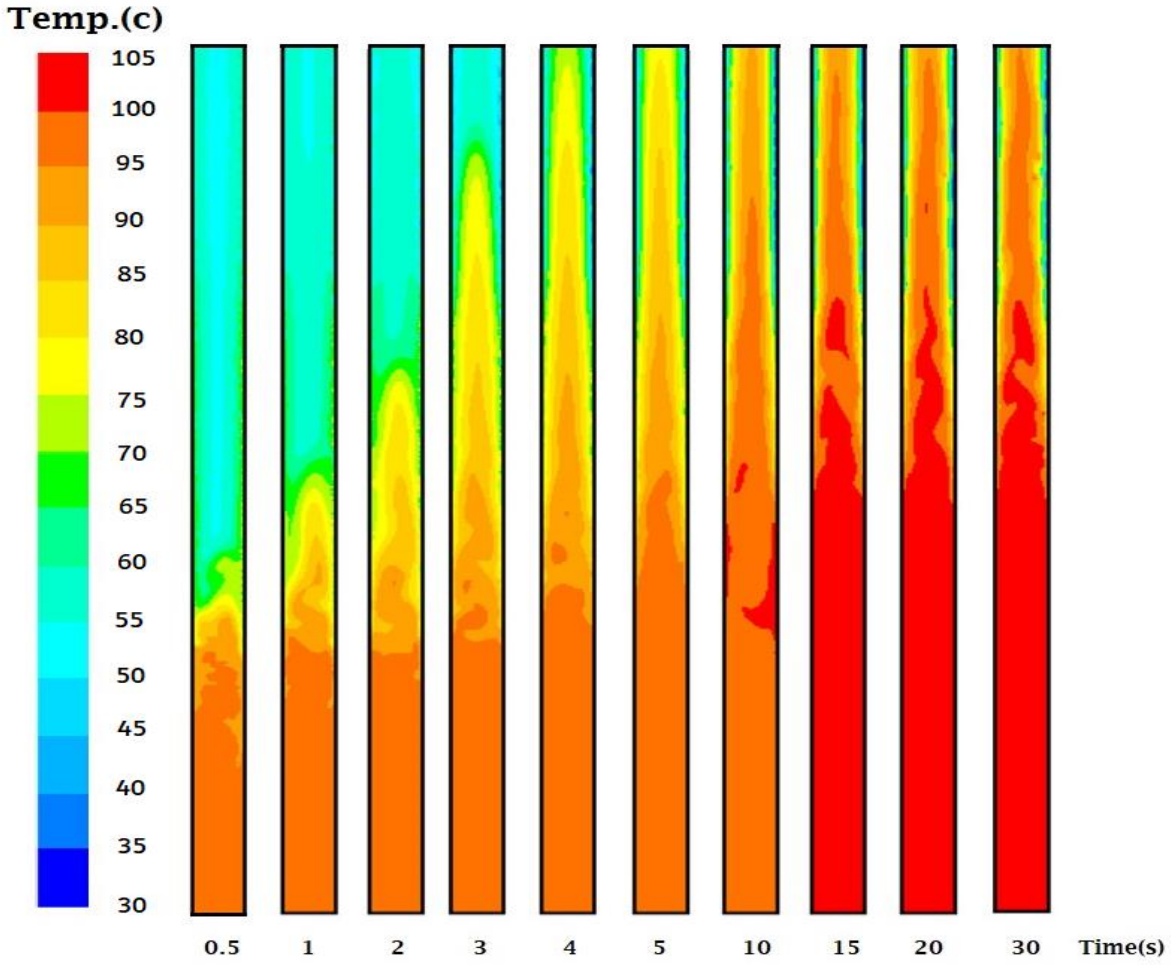

Figure 14. Temperature contours at different simulation times at a power input of 400 W, filling ratio of 65% and tilt angle of 90°.

5. Conclusions

The heat pipe thermosyphon is considered in this paper when charged with three filling ratios of working fluids (25%, 65%, and 100%) and three tilt angles (30°, 60°, and 90°) with different values of heat input (100, 200, 300, and 400 W). Numerical simulations of the evaporation and condensation phenomena inside the thermosyphon heat pipe are performed to study the effect of the filling ratio and tilt angle on the performance of the thermosyphon heat pipe in terms of thermal resistance. It is concluded that:

1. The thermosyphon was adequately modeled using a CFD simulation, and its thermal performance was examined in relation to filling ratio and inclination angle**.**
2. This study is validated in terms of the temperature distribution of thermosyphon wall for two input powers of 39W and 101W at filling ratio 65% and tilt angle of 90° with published numerical data at maximum deviations of 6.3%.
3. Thermal resistance decreases when the input power increases at all filling ratios and tilt angles.
4. The lowest thermal resistance and average temperature of the evaporator is at 65% filling ratio and 90° tilt angle, and its highest value is at 25% filling ratio and 30° tilt angle.
5. At a filling ratio of 65%, a tilt angle of 90°, and an input heat of 400 W, the vapor begins to form as bubbles at time of 1 second, and the vapor rises to the condenser section starting at time of 20 seconds.

References

[1] D. Reay, R. McGlen, and P. Kew, Heat pipes: theory, design and applications. Butterworth-Heinemann, 2013.

[2] A. Faghri, Heat pipe science and technology. Global Digital Press, 1995.

[3] M. Arab, M. Soltanieh, and M. B. Shafii, "Experimental investigation of extra-long pulsating heat pipe application in solar water heaters," Experimental Thermal and Fluid Science, vol. 42, pp. 6-15, 2012, doi: 10.1016/j.expthermflusci.2012.03.006.

[4] A. Ozsoy and V. Corumlu, "Thermal performance of a thermosyphon heat pipe evacuated tube solar collector using silver-water nanofluid for commercial applications," Renewable Energy, vol. 122, pp. 26-34, 2018, doi: 10.1016/j.renene.2018.01.031.

[5] Y.-C. Weng, H.-P. Cho, C.-C. Chang, and S.-L. Chen, "Heat pipe with PCM for electronic cooling," Applied Energy, vol. 88, no. 5, pp. 1825-1833, 2011, doi: 10.1016/j.apenergy.2010.12.004.

[6] W. Huang, W. Cao, and F. Jiang, "A novel single-well geothermal system for hot dry rock geothermal energy exploitation," Energy, vol. 162, pp. 630-644, 2018, doi: 10.1016/j.energy.2018.08.055.

[7] X. P. Wu, P. Johnson, and A. Akbarzadeh, "Application of heat pipe heat exchangers to humidity control in air-conditioning systems," Applied thermal engineering, vol. 17, no. 6, pp. 561-568, 1997.

[8] G. P. Peterson, "An introduction to heat pipes. Modeling, testing, and applications," Wiley Series in Thermal Management of Microelectronic and Electronic Systems, 1994.

[9] S. H. Noie, "Heat transfer characteristics of a two-phase closed thermosyphon," Applied Thermal Engineering, vol. 25, no. 4, pp. 495-506, 2005, doi: 10.1016/j.applthermaleng.2004.06.019.

[10] J. Raghuram, K. P. Kumar, G. Khiran, K. Snehith, and S. B. Prakash, "Thermal performance of a selected heat pipe at different tilt angles," in IOP Conference Series: Materials Science and Engineering, 2017, vol. 225, no. 1: IOP Publishing, p. 012043.

[11] B. Jiao, L. M. Qiu, X. B. Zhang, and Y. Zhang, "Investigation on the effect of fillinging ratio on the steady-state heat transfer performance of a vertical two-phase closed thermosyphon," Applied Thermal Engineering, vol. 28, no. 11-12, pp. 1417-1426, 2008, doi: 10.1016/j.applthermaleng.2007.09.009.

[12] A. A. Chehade, H. Louahlia-Gualous, S. Le Masson, I. Victor, and N. Abouzahab-Damaj, "Experimental investigation of thermosyphon loop thermal performance," Energy Conversion and Management, vol. 84, pp. 671-680, 2014, doi: 10.1016/j.enconman.2014.04.092.

[13] R. Manimaran, K. Palaniradja, N. Alagumurthi, and K. Velmurugan, "An Investigation of Thermal Performance of Heat Pipe Using Di-water," Science and Technology, vol. 2, no. 4, pp. 77-80, 2012, doi: 10.5923/j.scit.20120204.04.

[14] A. Alizadehdakhel, M. Rahimi, and A. A. Alsairafi, "CFD modeling of flow and heat transfer in a thermosyphon," International Communications in Heat and Mass Transfer, vol. 37, no. 3, pp. 312-318, 2010, doi: 10.1016/j.icheatmasstransfer.2009.09.002.

[15] L. Lu, Z.-H. Liu, and H.-S. Xiao, "Thermal performance of an open thermosyphon using nanofluids for high-temperature evacuated tubular solar collectors," Solar Energy, vol. 85, no. 2, pp. 379-387, 2011, doi: 10.1016/j.solener.2010.11.008.

[16] H. Arat, O. Arslan, U. Ercetin, and A. Akbulut, "Experimental study on heat transfer characteristics of closed thermosyphon at different volumes and inclination angles for variable vacuum pressures," Case Studies in Thermal Engineering, vol. 26, 2021, doi: 10.1016/j.csite.2021.101117.

[17] N. Ashgriz and J. Mostaghimi, "An introduction to computational fluid dynamics," Fluid flow handbook, vol. 1, pp. 1-49, 2002.

[18] A. Kumar, "Analysis of Heat Transfer and Fluid Flow in Different Shaped Roughness Elements on the Absorber Plate Solar Air Heater Duct," Energy Procedia, vol. 57, pp. 2102-2111, 2014, doi: 10.1016/j.egypro.2014.10.176.

[19] A. A. Alammar, R. K. Al-Dadah, and S. M. Mahmoud, "Numerical investigation of effect of fill ratio and inclination angle on a thermosiphon heat pipe thermal performance," Applied Thermal Engineering, vol. 108, pp. 1055-1065, 2016, doi: 10.1016/j.applthermaleng.2016.07.163.

[20] F. P. Incropera, D. P. DeWitt, T. L. Bergman, and A. S. Lavine, Fundamentals of heat and mass transfer. Wiley New York, 1996.

[21] A. A. G. Alammar, "Enhancing thermal performance of heat pipe based solar thermal collector," University of Birmingham, 2018.

[22] S. C. K. De Schepper, G. J. Heynderickx, and G. B. Marin, "Modeling the evaporation of a hydrocarbon feedstock in the convection section of a steam cracker," Computers & Chemical Engineering, vol. 33, no. 1, pp. 122-132, 2009, doi: 10.1016/j.compchemeng.2008.07.013.

[23] B. Fadhl, L. C. Wrobel, and H. Jouhara, "Numerical modelling of the temperature distribution in a two-phase closed thermosyphon," Applied Thermal Engineering, vol. 60, no. 1-2, pp. 122-131, 2013.

[24] M. Nazarimanesh, T. Yousefi, and M. Ashjaee, "Experimental study on the effects of inclination situation of the sintered heat pipe on its thermal performance," Experimental Thermal and Fluid Science, vol. 68, pp. 625-633, 2015.

[25] H. Jouhara and A. J. Robinson, "Experimental investigation of small diameter two-phase closed thermosyphons charged with water, FC-84, FC-77 and FC-3283," Applied thermal engineering, vol. 30, no. 2-3, pp. 201-211, 2010.

محاكاة عددية لخصائص انتقال الحرارة لأنبوب الحرارة ذو السيفون الحراري بزوايا ميل ونسب تعبئة مختلفة

الخلاصة: يمكن استخدام النمذجة الديناميكية الحسابية للسوائل لأنبوب الحرارة لدراسة الظواهر الفيزيائية المعقدة لعملية تغيير الطور أثناء التبخر والتكثيف في لإجراء محاكاة عددية للتدفق ثنائي الطور داخل أنبوب FLUENT (ANSYS 22) أنابيب الحرارة ذات السيفون الحراري. في هذه الدراسة تم استخدام حراري ذو سيفون حراري لدراسة تأثير كل من نسبة الملء وزاوية ميل الأنبوب الحراري على الأداء الحراري من حيث المقاومة الحرارية وتوزيع درجة الحرارة. وتمت مقارنة النتائج مع بحث منشور، حيث أظهرت توافقاً جيداً مع أعلى انحراف في توزيع درجات الحرارة بحوالي 6.3% وبحسب النتائج، عند نسبة تعبئة 65% ، كان متوسط درجة حرارة جدران المبخر في أدنى مستوياته، بينما عند نسبة تعبئة 25%، كان في أعلى مستوياته. عند جميع قيم المدخلات الحرارية، تم الوصول إلى أدنى مقاومة حرارية إجمالية عند زاوية ميل قدرها 90 درجة ونسبة تعبئة قدرها 65% تتناقص المقاومة الحرارية مع زيادة مدخلات الحرارة، كما تصبح تأثيرات نسبة الملء وزاوية الميل أكثر أهمية مع ارتفاع مدخلات الحرارة. بالإضافة إلى ذلك، عند مدخل حرارة 400 واط ، ونسبة تعبئة 65%، وزاوية ميل 90 درجة، تبدأ الفقاعات بالتشكل عند زمن 1 ثانية، ويرتفع البخار إلى قسم المكثف ابتداءً من زمن 20 ثانية، حاملاً معها الطاقة الحرارية. .بينما يبدأ التكثيف عند الزمن 27 ثانية.

الكلمات الدالة: المحاكاة العددية، الأنابيب الحرارية، السيفون الحراري، نسبة المل، زاوية الميل.